Solution Structure of the Vam7p PX Domain[†,‡]

Jun Lu,[§,||] Jesus Garcia,[§,||] Irina Dulubova,[§,||] Thomas C. Südhof,[⊥,@,#] and Josep Rizo*[,§,||]

Departments of Biochemistry, Pharmacology, and Molecular Genetics, Center for Basic Neuroscience, and Howard Hughes Medical Institute, University of Texas Southwestern Medical Center, 5323 Harry Hines Boulevard, Dallas, Texas 75390

Received January 17, 2002

ABSTRACT: PX domains have been recently found to act as phosphoinositide binding modules. In the yeast SNARE protein Vam7p, the PX domain binds to PtdIns(3)P and is required for vacuolar targeting. To gain insight into how PX domains function, the solution structure of the ligand-free Vam7p PX domain has been determined by NMR spectroscopy. The Vam7p PX domain has the same overall α/β fold observed in the structures of the ligand-free p47^{phox} PX domain and the PtdIns(3)P-bound p40^{phox} PX domain, exhibiting several similarities and differences with these two PX domains. Most striking is the similarity between the Vam7p and p40^{phox} PX domains in a subset of secondary structure elements despite the low level of sequence identity between them, suggesting that these elements form a conserved core in the PX domain fold. These similarities and the observation that a putative PtdIns(3)P binding site is already formed in the apo Vam7p PX domains suggest that ligand binding does not induce major conformational changes, contrary to what was previously thought. The proposed ligand binding site of the Vam7p PX domain includes basic side chains from the conserved structural core that also participate in PtdIns(3)P binding to the p40^{phox} PX domain, and basic side chains from a variable loop that probably inserts into the membrane. These results indicate that PX domains contain a combination of conserved and variable features that allow them to have a common function and at the same time exhibit distinct specificities, mechanisms of regulation, or modes of interaction with effector molecules.

Phosphoinositides are involved in the spatial and temporal regulation of a wide variety of cellular processes, playing key roles in the membrane recruitment and/or activation of proteins that control such processes (*1*−*3*). Major advances in understanding phosphoinositide signaling have arisen from the identification and characterization of several protein modules that specifically recognize these lipids, including the ENTH,[1] PH, FYVE, and FERM domains (*4*). An additional, versatile phosphoinositide-binding module, the PX domain, has emerged from a flurry of recent research (*5*, *6*). The PX domain was first identified in the p40^{phox} and p47^{phox} subunits of the NADPH oxidase through a search for sequences homologous to a region from the Cpk class of PI3 kinases (*7*), and more than 100 PX domain-containing proteins are currently found in eukaryotic genome databases (*8*). These proteins participate in a wide range of biological processes, including membrane traffic (e.g., Vam7p and sorting nexins), signal transduction (e.g., PI3K-C2, PLDs, and RGS-PX1), cell growth and survival (e.g., CISK), cytoskeleton organization (e.g., Bem1p), and neutrophil defense (e.g., p40^{phox} and p47^{phox}). Perhaps reflecting this functional diversity, the level of sequence similarity among PX domains is generally low. In addition, different PX domains exhibit different preferences and degrees of specificity for distinct phosphoinositides, although PtdIns(3)P is the most common target (*9*). Thus, while the PX domains of p40^{phox}, SNX3, SNX7, and Vam7p bind PtdIns(3)P with moderate to high specificity (*10*−*14*), the RGS-PX1 PX domain also binds to PtdIns(3)P but is rather promiscuous (*15*). On the other hand, the PX domains of Bem1p and PI3K-C2 bind specifically to PtdIns(4)P and PtdIns(4,5)P_2, respectively (*14*, *16*), whereas the p47^{phox} and CISK PX domains appear to have a broad preference for multiply phosphorylated phosphoinositides (*11*, *17*−*19*).

The solution structure of the p47^{phox} PX domain determined by NMR spectroscopy revealed a novel α/β fold with an exposed proline-rich loop that binds to the p47^{phox} SH3 domain (*20*). Another NMR study indicated that the Vam7p PX domain has a similar secondary structure, although its three-dimensional structure was not described (*13*). This study also suggested that phosphoinositide binding is mediated by five basic elements and involves substantial conformational changes. The crystal structure of the p40^{phox} PX domain bound to PtdIns(3)P provided the first view at atomic resolution of how phosphoinositides are recognized by PX

[†] This work was supported by a grant from the Welch Foundation and by NIH Grant NS37200.

[‡] The coordinates of the Vam7p PX domain were deposited in the Protein Data Bank (entry 1KMD) and the resonance assignments in the BioMagResBank (accession number 5385).

* To whom correspondence should be addressed. Telephone: (214) 648-9026. Fax: (214) 648-8673. E-mail: jose@arnie.swmed.edu.

[§] Department of Biochemistry.

[||] Department of Pharmacology.

[⊥] Department of Molecular Genetics.

[@] Center for Basic Neuroscience.

[#] Howard Hughes Medical Institute.

[1] Abbreviations: CISK, cytokine-independent survival kinase; ENTH, epsin N-terminal homology; FERM, band 4.1, ezrin, radixin, and moesin; FYVE, Fab1, YOTB, Vac1, and EEA1; NMR, nuclear magnetic resonance; PH, pleckstrin homology; Phox, phagocyte NADPH oxidase; PLD, phospholipase D; PtdIns, phosphatidylinositol; PtdIns(3)P, PtdIns 3-phosphate; PtdIns(4)P, PtdIns 4-phosphate; PtdIns(4,5)P_2, PtdIns 4,5-bisphosphate; PX, Phox homology; RGS, regulator of G protein signaling; SNX, sorting nexins.

10.1021/bi020050b CCC: $22.00
Published on Web 04/17/2002

domains and yielded critical insights into how specificity is achieved (*21*). This work also revealed drastic differences between the $p40^{phox}$ and $p47^{phox}$ PX domain structures in the phosphoinositide binding cleft, but it is unclear whether these differences arise because of the distinct specificities of the two domains, or are due to conformational changes induced by ligand binding. Assessing the significance of these and other structural differences between these two PX domains is further hindered by the lack of additional PX domain structures and by the generally low level of sequence similarity among PX domains. To shed light on these critical questions and gain further insights into how PX domains function, we have determined the three-dimensional structure of the PX domain from Vam7p using NMR spectroscopy. Our results reveal that PX domains share a structural core that lines the phosphoinositide binding site. In addition, we find that the binding site is already formed in the Vam7p PX domain, implying that ligand binding does not involve substantial backbone conformational changes.

MATERIALS AND METHODS

Sample Preparation. DNA encoding GST fusions of protein fragments that include the vam7p PX domain (residues 1−137 or 8−124) were amplified by PCR from full-length vam7p cDNA using custom-designed primers (Operon) and subcloned into pGEX-KG (*22*). The fusion proteins were expressed in *Escherichia coli* BL21-*cotonplus*-TM-DE3-TIL (Stratagene), affinity purified on glutathione sepharose (Pharmacia), treated with Benzonase Nuclease (Novagen), and cleaved with thrombin (Sigma). The eluted protein was further purified by cationic exchange chromatography at pH 6.2 on a monoS column (Pharmacia). Uniform ^{15}N labeling was achieved by growing the bacteria in $^{15}NH_4Cl$ (Isotec, Miamisburg, OH) as a sole source of nitrogen; for uniform labeling with ^{15}N and ^{13}C, [$^{13}C_6$]glucose (Isotec) was used as the sole source of carbon.

NMR Spectroscopy. All NMR experiments were carried out at 25 °C on Varian Inova500 or Inova600 spectrometers with samples dissolved in 20 mM Mes (pH 6.2). Samples of 0.5 mM ^{15}N-labeled and ^{15}N- and ^{13}C-labeled Vam7p fragment containing the PX domain (residues 8−124) were used to determine the structure using a suite of pulsed-field gradient-enhanced NMR experiments (*23*−*26*). Briefly, these included three-dimensional (3D) $^1H-^{15}N$ TOCSY-HSQC, HNCO, HNCACB, CBCA(CO)NH, (H)CBCACO(CA)HA, (H)C(CO)NH-TOCSY, H(C)(CO)NH-TOCSY, and HCCH-TOCSY spectra for resonance assignments, and two-dimensional (2D) NOESY, 3D $^1H-^{15}N$ NOESY-HSQC, and 3D $^1H-^{13}C$ NOESY-HSQC experiments carried out with mixing times of 100 ms to measure NOEs for structure determination. Protection of amide protons from the solvent was assessed from the intensities of exchange cross-peaks with the water resonance in 3D $^1H-^{15}N$ TOCSY-HSQC experiments. Stereospecific assignments of Val and Leu methyl groups were obtained from a $^1H-^{13}C$ HSQC spectrum acquired on a 0.5 mM sample of 10% ^{13}C-labeled PX domain. All data were processed with the program NMRPipe (*27*) and analyzed with the program NMRView (*28*).

Structure Calculations. NOE cross-peak intensities were classified as strong, medium, weak, and very weak, and assigned to restraints of 1.8−2.8, 1.8−3.5, 1.8−5.0, and 1.8−6.0 Å, respectively, with appropriate pseudoatom corrections. ϕ and ψ torsion angle restraints were included on the basis of analysis of HN, ^{15}N, $^{13}C\alpha$, ^{13}CO, and $^{13}C\beta$ chemical shifts using the program TALOS (*29*). Dihedral angles were restrained to the maximum of 22.5° or 1.5 times the standard deviation observed in the TALOS database matches. To restrain hydrogen bonds, the H−O distances were restrained to 1.3−2.5 Å and the N−O distances to 2.3−3.5 Å. Structures of the PX domain were calculated by simulated annealing using torsion angle dynamics with the program CNS (*30*). A total of 500 structures were calculated with the final set of restraints, and the 20 structures with the lowest NOE energy were selected.

RESULTS

Solution Structure of the Vam7p PX Domain. Vam7p is a SNARE protein that functions in vacuolar membrane traffic in yeast (*31*), participating in formation of the SNARE complex that is critical for membrane fusion (*32*). The sequence of Vam7p contains (i) an N-terminal PX domain that binds to PtdIns(3)P and is required for localization to the vacuole (*13*), (ii) a linker region, and (iii) a C-terminal SNARE motif. To define the boundaries of the PX domain, we initially analyzed a fragment containing residues 1−137 of Vam7p by NMR spectroscopy and found that the fragment contained a properly folded domain but had a strong tendency to aggregate over time. Partial resonance assignment of this fragment revealed that residues 11−121 form a structured domain while the remaining sequences at the N- and C-termini are unstructured. Hence, we prepared a smaller fragment (residues 8−124) that included the structured region. This fragment also had a tendency to aggregate over time but was stable for weeks at 25 °C in 20 mM MES (pH 6.2) when the protein concentration was kept below 0.5 mM. We thus determined the three-dimensional structure of the $Vam7p^{8-124}$ fragment under these conditions using multidimensional heteronuclear NMR experiments.

The final structure calculations of the Vam7p PX domain were performed using a set of 1443 unique, conformationally significant experimental restraints. A backbone superposition of the 20 structures with the lowest NOE energies is shown in Figure 1A, and the structural statistics are summarized in Table 1. The structures are characterized by good Ramachandran map statistics, as well as by low deviations from the experimental restraints and from idealized covalent geometry. The Vam7p PX domain solution structure is generally well-defined except for a long loop that contains the proline-rich region. The observation that this region is characterized by sharp resonances, a lack of protection of amide groups against exchange with the solvent, and an absence of long-range NOEs showed that this loop is highly flexible. The ribbon diagram of a representative conformer of the Vam7p PX domain shown in Figure 1B illustrates that the structure can be divided into two parts or subdomains, an N-terminal β-sheet and a C-terminal helical bundle, that pack against each other. The β-sheet contains three antiparallel β-strands connected by tight turns, while the helical subdomain includes two main α-helices (α1 and α2) connected by the flexible proline-rich loop and a third helical sequence that is bent in the middle (α3−α3′).

PX Domains Contain a Conserved Structural Core. The overall fold of the Vam7p PX domain is analogous to that

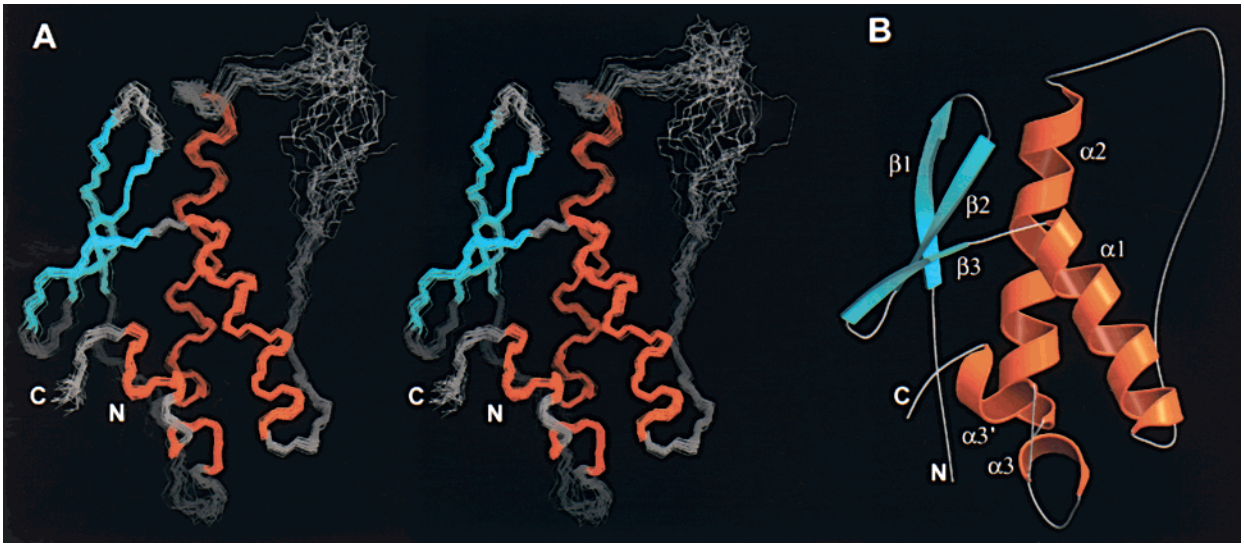

FIGURE 1: Three-dimensional structure of the Vam7p PX domain. (A) Stereo backbone superposition of the 20 structures of the Vam7p PX domain with the lowest NOE energies. (B) Ribbon diagram of the Vam7p PX domain. The β-strands (cyan) and the α-helices (orange), as well as the N- and C-termini, have been labeled with the same nomenclature used in Figure 2. This figure was generated with the programs InsightII (MSI, San Diego, CA) and Molscript (*35*).

Table 1: Structural Statistics for the 20 Structures of the Vam7p PX Domain with the Lowest NOE Energies[a]

Average Rmsds from Experimental Restraints (1443 total)		
NOE distance restraints (Å)		
all	1193	0.0048 ± 0.0004
intraresidue	314	0.0058 ± 0.0011
sequential ($i - j = 1$)	348	0.0046 ± 0.0009
short-range ($i - j = 2-4$)	185	0.0053 ± 0.0010
long-range ($i - j > 4$)	346	0.0034 ± 0.0005
hydrogen bonds (Å)	98	0.0022 ± 0.0008
dihedral angels (deg)	152	0.058 ± 0.0086
Average Rmsds from Idealized Covalent Geometry		
bonds (Å)		0.001 ± 0.00001
angles (deg)		0.30 ± 0.004
impropers (deg)		0.11 ± 0.0056
Ramachandran Plot Statistics (%)[b]		
residues in most favored region		83.5
residues in additionally allowed region		15.2
residues in generously allowed region		1.0
residues in nonallowed region		0.7
Rmsds from the Average Structure		
backbone residues (14−64 and 80−119)		0.46
heavy atom residues (14−64 and 80−119)		1.09
all backbone residues (11−121)		0.86
all heavy atom residues (11−121)		1.48

[a] All 20 structures have NOE energies of <10 kcal/mol. There were no NOE violations larger than 0.2 Å or dihedral angle violations larger than 2°. [b] Calculated using the program Procheck (*34*).

observed for the PX domains from p47^{phox} (*20*) and p40^{phox} (*21*), although there are a number of differences in their secondary structure elements. These differences are summarized in Figure 2 together with a sequence alignment of the three PX domains based on pairwise structural superpositions obtained with the program DALI (*33*)[2] (see Figure 3). Using all conformers from the NMR ensembles, the average root-mean-square (rms) deviations yielded by DALI were 2.8 Å for the Vam7p/p40^{phox} pair (99 equivalent Cα atoms), 3.4 Å for the Vam7p/p47^{phox} pair (91 equivalent Cα atoms),

[2] For a more comprehensive alignment of PX domain sequences, see ref *6* or *7*.

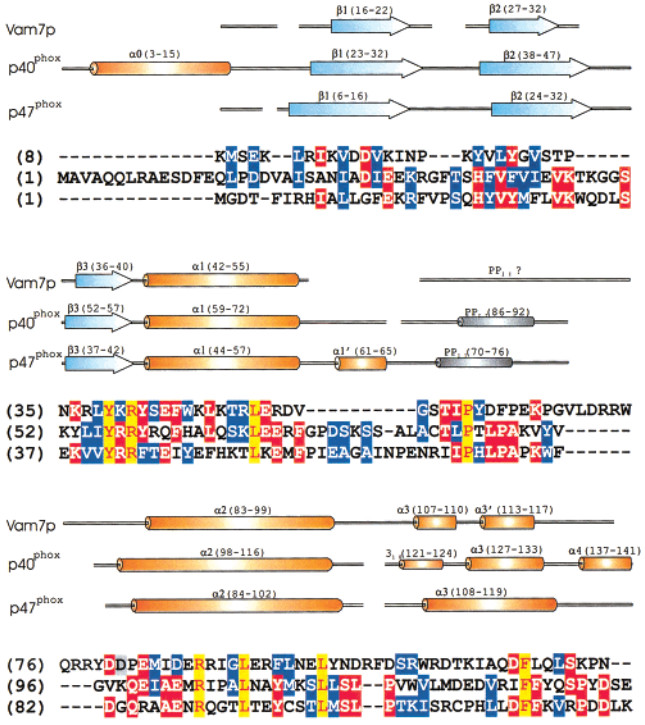

FIGURE 2: Comparison of the sequence and secondary structure of the Vam7p PX domain with those of the p40^{phox} and p47^{phox} PX domains. A sequence alignment of the three PX domains based on structural superpositions obtained with the program DALI (*33*) is shown, with the following color code: red letters with yellow background, identical in the three PX domains; white letters with red background, identical in two PX domains; and white letters with blue background, conserved but not identical residues. A summary of the observed secondary structure elements is shown above the sequence. The numbering system used to designate the secondary structure elements has been adapted to facilitate comparison among the three PX domains. Arrows represent β-strands, and cylinders represent helices. In p40^{phox} and p47^{phox}, a short, proline-rich sequence forms a polyproline II helix that is not strictly conserved in Vam7p, although a few residues in the homologous positions do have torsion angles characteristic of a polyproline II helix.

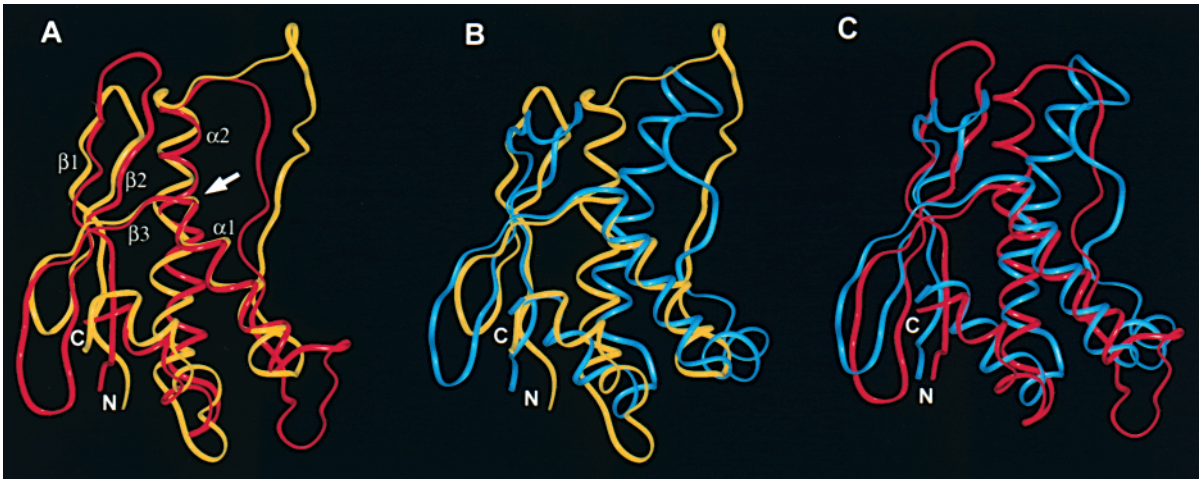

FIGURE 3: Superpositions of representative conformers of the Vam7p, p40^{phox}, and p47^{phox} PX domains obtained with the program DALI (*33*): (A) Vam7p (yellow) vs p40^{phox} (red), (B) Vam7p (yellow) vs p47^{phox} (blue), and (C) p40^{phox} (red) vs p47^{phox} (blue). The orientation used in all superpositions is similar to that shown for Vam7p in Figure 1. The white arrow in panel A points to the highly conserved sequence in the corner between strand β3 and helix α1, which lines the phosphoinositide binding site. This figure was generated with the program InsightII (MSI, San Diego, CA).

and 3.6 Å for the p40^{phox}/p47^{phox} pair (107 equivalent Cα atoms). These relatively large deviations arise in part from the low level of sequence homology among these PX domains (11, 11, and 22%, respectively), and in particular from the divergence of the proline-rich loop. Indeed, a much closer structural similarity in a core of secondary structure elements, which include the three β-strands and helices α1 and α2, is clearly apparent in the superposition of the Vam7p and p40^{phox} PX domains (Figure 3A). The average rms deviation between these two PX domains when only this core is superimposed is 1.3 Å for 42 equivalent Cα atoms. The structural resemblance of the β-sheet is particularly remarkable considering the low level of sequence similarity in this region and the different length of the connecting loops (Figures 2 and 3A), and includes a β-bulge in strand 1 (residues Asp^{18} and Asp^{19} of the Vam7p PX domain).[3] The center of the structural core is formed by the corner between strand β3 and helix α1 (indicated by the white arrow in Figure 3A), which exhibits the highest level of sequence conservation in PX domains (see Figure 2 and ref *6*) and includes residues that are critical for phosphoinositide binding (ref *21* and see below). These observations support the notion that phosphoinositide binding constitutes the primary function of PX domains.

The structure described for the p47^{phox} PX domain is most similar to those of the Vam7p and p40^{phox} PX domains in the structural core but, surprisingly, exhibits a conspicuous difference in the orientation of the N-terminal half of helix α2 (Figure 3B,C). This different orientation suggested a large ligand-induced conformational change when the structures of the apo p47^{phox} and holo p40^{phox} PX domains were compared (see ref *21*), and results in a dramatically different shape right above the phosphoinositide binding site (Figure 4). In the structures of the Vam7p and p40^{phox} PX domains, the N-terminal part of helix α2 and a few preceding residues are well packed against the loop connecting strands β1 and β2 (Figure 4A,B). However, these two regions do not make contact in the structure of the p47^{phox} PX domain, resulting in a deep cleft above the location of the phosphoinositide binding site. These observations are surprising since several of the residues involved in the packing interactions between these two regions in p40^{phox} (F39, F41, Q99, A102, E103, and R105) are conserved in the p47^{phox} PX domain (Figure 2). These differences could in principle be due to a ligand-induced conformational change, but it is also plausible that the interface between these two regions could not be well-defined in the structure of the p47^{phox} PX domain because long-range NOEs between protons in these two regions could not be identified. Indeed, the similarity between the structures of the ligand-free Vam7p PX domain and the ligand-bound p40^{phox} PX domain in this region suggests that ligand binding does not cause substantial backbone conformational changes (see below for additional details).

Phosphoinositide Binding Site in the Vam7p PX Domain. The three-dimensional structure of the apo Vam7p PX domain described here, together with the ligand-induced chemical shift changes described by Overduin and co-workers (*13*), offers an opportunity to examine how this PX domain binds to PtdIns(3)P and to compare the binding site with that observed in the p40^{phox} PX domain (*21*). Figure 5 shows a ribbon diagram of a representative conformer of the Vam7p PX domain together with a ball-and-stick model of PtdIns(3)P obtained from the crystal structure of the p40^{phox} PX domain and placed according to the DALI superposition from Figure 3A. The positions of the 10 residues whose backbone amide protons exhibit the largest chemical shift changes upon binding to dibutanoyl PtdIns(3)P (*13*) have been colored in orange on the ribbon diagram. All these backbone amide groups are located around the putative PtdIns(3)P binding site, showing that its location in the Vam7p PX domain indeed coincides with that observed in the p40^{phox} PX domain. Superposition of the 20 structures of the Vam7p PX domain with the crystal structure of the p40^{phox} PX domain revealed five basic side chains (R41, K47, K67, R77, and R88) that point toward the ligand in at least some of the structures. All these side chains exhibit high

[3] Note that the presence of this bulge led to the previous conclusion that the Vam7p PX domain contains four β-strands, rather than three, based on chemical shift analysis (*13*).

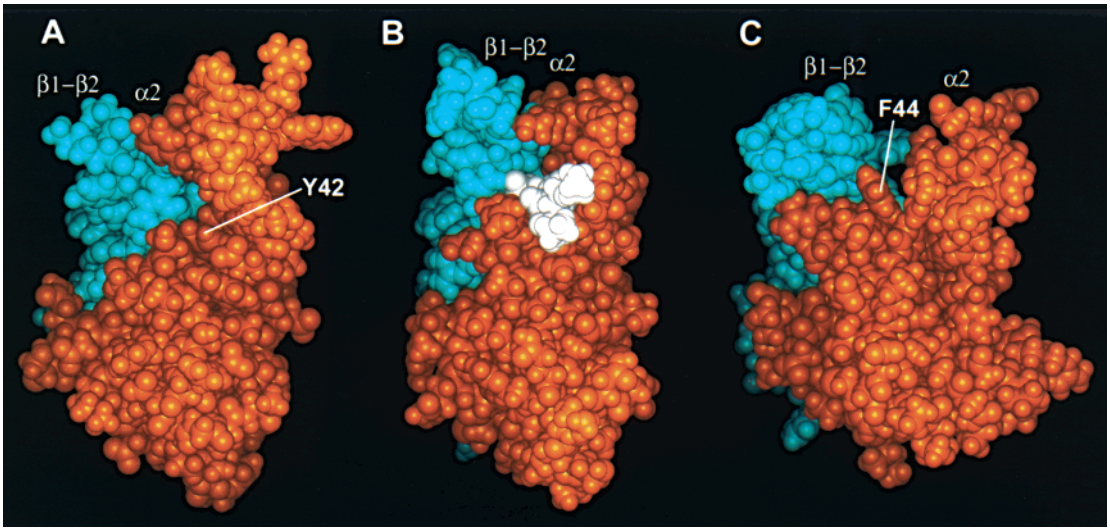

FIGURE 4: Space-filling models of the Vam7p (A), p40^{phox} (B), and p47^{phox} (C) PX domains. Atoms from the N-terminal β-sheet subdomain are colored in cyan, and those from the C-terminal helical bundle domain are colored in orange. The ligand is shown in white for the p40^{phox} PX domain. The structures have an orientation similar to those used in Figures 1 and 3, but are slightly rotated around the *y* axis to allow a better appreciation of the packing between the $\beta1-\beta2$ loop and the N-terminus of helix $\alpha2$ at the top of the domain. The side chains of Y42 in Vam7p and F44 in p47^{phox} are labeled. This figure was generated with the program InsightII (MSI, San Diego, CA).

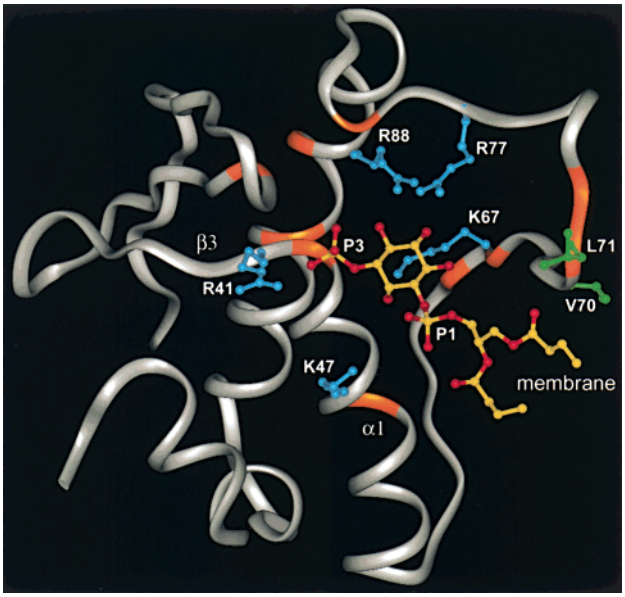

FIGURE 5: Model of the PtdIns(3)P binding site of the Vam7p PX domain. A ribbon diagram of a representative conformer of the Vam7p PX domain is shown in gray with the positions of the 10 residues whose amide groups exhibit largest chemical shift changes upon binding to dibutanoyl PtdIns(3)P (*13*) colored in orange. A ball-and-stick model of PtdIns(3)P from the structure of the p40^{phox} domain (*21*) is shown in the location resulting after superimposition of the structures of the two PX domains (oxygen atoms colored in red and other atoms colored in yellow). The approximate location of the membrane is indicated. The side chains of five basic side chains that point to the PtdIns(3)P binding site in selected conformers of the Vam7p PX domain are shown as blue ball-and-stick models. All these side chains are flexible but are displayed in these particular conformations found in selected conformers to illustrate the fact that they can easily coordinate the ligand without needing substantial conformational changes in the backbone. Two hydrophobic residues in the loop sequence formed by residues 70−77 are shown as green ball-and-stick models to illustrate their proximity to the acyl chains from the ligand and the likelihood that these side chains may insert into the membrane. This figure was generated with the program InsightII (MSI, San Diego, CA).

flexibility in the structure of the Vam7p PX domain, but the ball-and-stick models of these five side chains in the conformations found in selected conformers (Figure 5) illustrate the fact that they can easily interact with the ligand without significant changes in the backbone conformation.

The Vam7p R41 and R88 side chains are conserved in many PX domains, and the homologous residues of p40^{phox} (R58 and R105) are involved in coordinating the 3-phosphate and the 4- and 5-hydroxyl groups of PtdIns(3)P, respectively (*21*). Figure 5 shows that these side chains are ideally positioned to play the same role in the Vam7p PX domain. On the other hand, the basic side chains that interact with the 1-phosphate group of PtdIns(3)P in the p40^{phox} PX domain (R60 and K92) are not conserved in Vam7p, but the K47 and K67 side chains of Vam7p can easily occupy the same geometrical positions and can thus play analogous roles in ligand binding. It is less clear whether the Vam7p R77 side chain is involved in ligand binding since no basic residue from the p40^{phox} PX domain coordinates PtdIns(3)P from an analogous position, but its presence may explain the finding that the Vam7p PX domain exhibits some low affinity for phosphoinositides containing a 5-phosphate group (*13*, *14*).

In addition to R41, the highly conserved K^{40}R^{41}Y^{42} sequence contains an aromatic residue that was shown to be critical for PtdIns(3)P binding to the Vam7p PX domain (*13*) and forms a stacking interaction with the inositol ring in the crystal structure of the p40^{phox} PX domain (*21*). The observation that the corresponding residue has a different orientation in the structure of the p47^{phox} PX domain and would block ligand binding (see Figure 4C) reinforced the notion that ligand binding to PX domains may require a substantial conformational change (see ref *21*). However, in the structure of the Vam7p PX domain, Y42 is properly positioned to easily establish the same stacking interaction with the inositol ring and has the same rotameric state observed in the p40^{phox} PX domain, rather than populating the unusual rotameric state observed in the p47^{phox} PX domain (*20*). Hence, all our data indicate that the ligand binding site is basically formed in the apo PX domain from Vam7p, and ligand binding should not require substantial

rearrangements in the backbone conformation. The small magnitude of most of the NH chemical shift changes observed upon binding of dibutanoyl PtdIns(3)P to the Vam7p PX domain (*13*) strongly supports this view. Only the relatively large chemical shift change in the E66 NH group appears to suggest a significant local rearrangement since the other NH group with a relatively large shift (Y42 NH) (*13*) is very likely to form a hydrogen bond with the 3-phosphate group of the ligand, as observed in the crystal structure of the p40^{phox} PX domain (*21*). Finally, it is worth noting that the loop sequence spanning residues 70−77 of Vam7p was proposed to insert into the membrane upon phosphoinositide binding (*13*), and the binding model of Figure 5 shows that, indeed, hydrophobic residues in this region could easily interact with the acyl chains without major changes in the backbone conformation.

DISCUSSION

Extensive research has recently established PX domains as novel phosphoinositide binding modules. Biophysical studies yielded the structure of two PX domains and the phosphoinositide binding mode for one of them, but critical questions remained about which structural features are shared among PX domains and about the structural consequences of ligand binding. The structure of the Vam7p PX domain described here provides a third three-dimensional structure for a member of this diverse family and shows that, while there are substantial structural differences among PX domains due to a generally low level of sequence similarity and the presence of insertions in the least conserved sequences, there is a conserved structural core formed by a three-stranded antiparallel β-sheet and two α-helices. The finding that this core is very similar in the Vam7p and p40^{phox} PX domains despite the low level of sequence similarity between them suggests that this core is highly conserved in all PX domains. In addition, the fact that this similarity is observed between a ligand-free and a ligand-bound PX domain suggests that ligand binding does not cause major structural rearrangements. This conclusion is strongly supported for the Vam7p PX domain by the small magnitude of the amide chemical shift changes induced by ligand binding (*13*), and by the observation that the ligand binding site is already formed in the three-dimensional structure described here. Further experimentation will be required to test whether this is a general property of the PX domain family, and in particular, it will be important to determine whether the differences observed in the orientation of helix α2 in the p47^{phox} PX domain arise from a paucity of long-range NOE data or reflect a true divergence in the mechanism of ligand binding by PX domains.

The structural comparisons presented here show that the center of the structural core of PX domains is formed by the corner between strand β3 and helix α1, which contains the most highly conserved sequence of the PX domain family. This sequence is critical for phosphoinositide binding, supporting the general view that this constitutes the primary activity of PX domains. Mapping the ligand-induced chemical shift changes (*13*) onto our structure of the Vam7p PX domain showed that the phosphoinositide binding site is in the same location observed for the p40^{phox} PX domain (*21*). This site is surrounded by a highly conserved surface and a variable surface formed by the long loop connecting helices α1 and α2. Correspondingly, the model for PtdIns(3)P binding to the Vam7p PX domain proposed in Figure 5 includes two highly conserved basic residues (Arg41 and Arg88) that are also involved in PtdIns(3)P binding to the p40^{phox} PX domain, and additional basic residues that are less conserved. This variability in the binding sites of PX domains may underlie differences in specificity, in the regulation of phosphoinositide binding, or in interactions with effector molecules. The currently intense research in this field will undoubtedly shed new light on these issues soon.

SUPPORTING INFORMATION AVAILABLE

^{1}H, ^{13}C, and ^{15}N chemical shifts of the Vam7p PX domain at pH 6.2 and 25 °C. This material is available free of charge via the Internet at http://pubs.acs.org.

REFERENCES

1. Martin, T. F. (1998) *Annu. Rev. Cell Dev. Biol. 14*, 231−264.
2. Fruman, D. A., Rameh, L. E., and Cantley, L. C. (1998) *Annu. Rev. Biochem. 67*, 481−507.
3. Odorizzi, G., Babst, M., and Emr, S. D. (2000) *Trends Biochem. Sci. 25*, 229−235.
4. Cullen, P. J., Cozier, G. E., Banting, G., and Mellor, H. (2001) *Curr. Biol. 11*, R882−R893.
5. Sato, T. K., Overduin, M., and Emr, S. D. (2001) *Science 294*, 1881−1885.
6. Xu, Y., Seet, L. F., Hanson, B., and Hong, W. (2001) *Biochem. J. 360*, 513−530.
7. Ponting, C. P. (1996) *Protein Sci. 5*, 2353−2357.
8. Schultz, J., Copley, R. R., Doerks, T., Ponting, C. P., and Bork, P. (2000) *Nucleic Acids Res. 28*, 231−234.
9. Yu, J. W., and Lemmon, M. A. (2001) *J. Biol. Chem. 276*, 44179−44184.
10. Ellson, C. D., Gobert-Gosse, S., Anderson, K. E., Davidson, K., Erdjument-Bromage, H., Tempst, P., Thuring, J. W., Cooper, M. A., Lim, Z. Y., Holmes, A. B., Gaffney, P. R., Coadwell, J., Chilvers, E. R., Hawkins, P. T., and Stephens, L. R. (2001) *Nat. Cell Biol. 3*, 679−682.
11. Kanai, F., Liu. H., Field, S. J., Akbary, H., Matsuo, T., Brown, G. E., Cantley, L. C., and Yaffe, M. B. (2001) *Nat. Cell Biol. 3*, 675−678.
12. Xu, Y., Hortsman, H., Seet, L., Wong, S. H., and Hong, W. (2001) *Nat. Cell Biol. 3*, 658−666.
13. Cheever, M. L., Sato, T. K., de Beer, T., Kutateladze, T. G., Emr, S. D., and Overduin M. (2001) *Nat. Cell Biol. 3*, 613−618.
14. Song, X., Xu, W., Zhang, A., Huang, G., Liang, X., Virbasius, J. V., Czech, M. P., and Zhou, G. W. (2001) *Biochemistry 40*, 8940−8944.
15. Zheng, B., Ma, Y. C., Ostrom, R. S., Lavoie, C., Gill, G. N., Insel, P. A., Huang, X. Y., and Farquhar, M. G. (2001) *Science 294*, 1939−1942.
16. Virbasius, J. V., Song, X., Pomerleau, D. P., Zhan, Y., Zhou, G. W., and Czech, M. P. (2001) *Proc. Natl. Acad. Sci. U.S.A. 98*, 12908−12913.
17. Ago, T., Takeya, R., Hiroaki, H., Kuribayashi, F., Ito, T., Kohda, D., and Sumimoto, H. (2001) *Biochem. Biophys. Res. Commun. 287*, 733−738.
18. Xu, J., Liu, D., Gill, G., and Songyang, Z. (2001) *J. Cell Biol. 154*, 699−705.
19. Zhan, Y., Virbasius, J. V., Song, X., Pomerleau, D. P., and Zhou, G. W. (2001) *J. Biol. Chem.* (in press).
20. Hiroaki, H., Ago, T., Ito, T., Sumimoto, H., and Kohda, D. (2001) *Nat. Struct. Biol. 8*, 526−530.
21. Bravo, J., Karathanassis, D., Pacold, C. M., Pacold, M. E., Ellson, C. D., Anderson, K. E., Butler, P. J., Lavenir, I., Perisic, O., Hawkins, P. T., Stephens, L., and Williams, R. L. (2001) *Mol. Cell 8*, 829−839.

22. Guan, K. L., and Dixon, J. E. (1991) *Anal. Biochem. 192*, 262−267.
23. Kay, L. E. (1993) *J. Am. Chem. Soc. 115*, 2055−2057.
24. Kay, L. E., Xu, G. Y., Singer, A. U., Muhandiram, D. R., and Formankay, J. D. (1993) *J. Magn. Reson., Ser. B 101*, 333−337.
25. Kay, L. E., Xu, G. Y., and Yamazaki, T. (1994) *J. Magn. Reson., Ser. A 109*, 129−133.
26. Muhandiram, D. R., and Kay, L. E. (1994) *J. Magn. Reson., Ser. B 103*, 203−216.
27. Delaglio, F., Grzesiek, S., Vuister, G. W., Zhu, G., Pfeifer, J., and Bax, A. (1995) *J. Biomol. NMR 6*, 277−293.
28. Johnson, B. A., and Blevins, R. A. (1994) *J. Biomol. NMR 4*, 603−614.
29. Cornilescu, G., Delaglio, F., and Bax, A. (1999) *J. Biomol. NMR 13*, 289−302.
30. Brünger, A. T., Adams, P. D., Clore, G. M., DeLano, W. L., Gros, P., Grosse-Kunstleve, R. W., Jiang, J., Kuszewski, J., Nilges, M., Pannu, N. S., Read, R. J., Rice, L. M., Simonson, T., and Warren, G. L. (1998) *Acta Crystallogr. D54*, 905−921.
31. Ungermann, C., and Wickner, W. (1998) *EMBO J. 17*, 3269−3276.
32. Jahn, R., and Südhof, T. C. (1999) *Annu. Rev. Biochem. 68*, 863−911.
33. Holm, L., and Sander, C. (1993) *J. Mol. Biol. 233*, 123−138.
34. Laskowski, R. A., MacArthur, M. W., Moss, D. S., and Thornton, J. M. (1993) *J. Appl. Crystallogr. 26*, 283−291.
35. Kraulis, P. J. (1991) *J. Appl. Crystallogr. 24*, 946−950.

BI020050B